Subspace-Based Estimation of Time Delays and Doppler Shifts

Andreas Jakobsson, A. Lee Swindlehurst, *Member, IEEE,* and Petre Stoica, *Fellow, IEEE*

***Abstract*—This paper considers the problem of estimating the time delays and Doppler shifts of a known waveform received via several distinct paths by an array of antennas. The general maximum likelihood estimator is presented, and is shown to require a $2d$-dimensional nonlinear minimization, where d is the number of received signal reflections. Two alternative solutions based on signal and noise subspace fitting are proposed, requiring only a d-dimensional minimization. In particular, we show how to decouple the required search into a two-step procedure, where the delays are estimated and the Dopplers solved for explicitly. Initial conditions for the time delay search can be obtained by applying generalizations of the MUSIC and ESPRIT algorithms, which are also outlined in the paper. Simulation examples are included to illustrate the algorithms' performance relative to the Cramér–Rao bound.**

***Index Terms*—Array signal processing, delay estimation, mobile communications, multipath channels, radar signal processing, subspace fitting.**

I. Introduction

THE PROBLEM of using an antenna array to estimate the time delays and Doppler shifts (or frequency offsets) of a known signal is important in two common applications. First, in active radar and sonar, a known waveform is transmitted, and reflections from objects "illuminated" by the transmission are subsequently received. The received signals are often modeled as scaled, delayed, and Doppler-shifted versions of the transmitted signal. Estimation of the signal amplitude, delay, and Doppler shift provides information about the position and relative motion of the objects.

The second application involves estimation of the parameters of a multipath communication channel in situations where the transmitter is rapidly moving or has an unknown frequency offset. For example, consider a situation where a remote mobile user transmits a known waveform (e.g., a training sequence) to a base station for synchronization or equalization purposes. If the channel is frequency selective (nonzero delay spread), then the signal will be received with several distinct delays. In addition, due to the motion of the mobile and variations in the carrier frequency of the transmitter, the known signal can also be received with a small frequency offset. Estimation of the delays and frequency offsets, as well as the spatial signatures of the signal arrivals, is necessary in establishing a clean, intersymbol, and interference-free communication link.

This paper presents a novel approach to solving the problems described above. The techniques presented are applicable in situations involving multiple antennas and, unlike classical methods, are asymptotically optimal at high SNR even when multiple overlapping copies of the signal are received. The frequency domain model used in [1] and [2] for time-delay estimation is generalized to incorporate the presence of (small) frequency offsets. The resulting *signal manifold* in the frequency domain is shown to be a generalized version of the signal manifold of [1] and [2] in much the same way that polarization [3]–[5] and local scattering [6] generalize the standard *array manifold* in direction-of-arrival (DOA) estimation. This observation motivates the development of subspace-based techniques similar to those in [4]–[6], which provide closed-form solutions for the linear parameters (in our case, the frequency/Doppler offsets). The resulting algorithms require a search for the time delays, but it is shown that for small frequency offsets, the closed-form time-delay estimation techniques of [1] and [2] provide excellent initial conditions.

Classical approaches to time-delay and Doppler estimation are based on matched filtering (see, e.g., [7], [8]). These techniques typically assume one signal path and one sensor, although the extension to multiple sensors is straightforward. Matched filtering techniques are known to be optimal in the maximum likelihood (ML) sense for a single signal arrival but are not consistent when multiple overlapping copies of the signal are present. While a number of authors have proposed time-delay estimators that exploit frequency domain data models, their use in Doppler estimation has not been widespread. When such models have been used, they have again only focused on the single signal path case [9], [10]. Other recently proposed techniques for the case of a single signal arrival include the wideband ambiguity function method of [11] and the structured covariance estimator of [12]. A recent paper [13] presents a deconvolution approach for resolving multiple delayed and Doppler shifted paths but only over a quantized parameter grid. The key features of the methods proposed below are that 1) they provide continuous-valued estimates of time delays and Doppler shifts for multiple signal arrivals, and 2) they are parametric estimators with asymptotic accuracy equivalent to that of the maximum likelihood approach.

Manuscript received September 8, 1997; revised March 4, 1998. This work was supported in part by the Swedish Institute, the Swedish Foundation for Strategic Research (SSF) through the Senior Individual Grant Program, the National Science Foundation under Grant MIP-9408154, and by the Office of Naval Research under Grant N00014-96-1-0934. The associate editor coordinating the review of this paper and approving it for publication was Prof. Pierre Comon.

A. Jakobsson and P. Stoica are with the Systems and Control Group, Department of Technology, Uppsala University, Uppsala, Sweden.

A. L. Swindlehurst is with the Department of Electrical and Computer Engineering, Brigham Young University, Provo, UT 84602 USA.

Publisher Item Identifier S 1053-587X(98)05959-5.

The outline of the paper is as follows. In the next section, we present time and frequency domain versions of the data model assumed in this work. By interchanging the roles of the samples in space and time, we show how the time delay and Doppler estimation problem can be cast in the well-studied framework of DOA estimation. In particular, we draw parallels between the array manifold in space that arises in DOA estimation and the signal manifold in time that we employ in this work. Under this paradigm, the classical matched filtering approach is seen to be equivalent to the simple delay-and-sum beamformer. Section III then presents the ML solution to the multiple sensor, multiple signal arrival problem and outlines the corresponding Cramér–Rao bound. The ML solution is shown to require, in general, a search over both the delay and Doppler parameters and may thus be difficult to implement in practice. For this reason, two asymptotically equivalent (in SNR) subspace fitting algorithms are derived in Section IV. These algorithms exploit the fact that to first order, the signal in the frequency domain depends on the Doppler frequency in a linear fashion, and hence, the Doppler may be estimated explicitly. A search is still required for the time delays, but this can be conveniently initialized by two suboptimal algorithms based on MUSIC [3] and ESPRIT [14] that are also presented. Finally, Section V provides the results of a number of simulation examples to illustrate the relative performance of the proposed algorithms.

II. Modeling

A. Assumptions

Suppose an m-element antenna array receives several scaled, time-delayed, and frequency/Doppler-shifted copies of a known baseband signal $s(t)$. The received signals could, for instance, be the echoes from a pulse transmitted by an active radar, or they could result from a training sequence sent over a multipath communication channel. In either case, we may model the output of the array for small frequency/Doppler offsets as

$$\mathbf{x}(t) = \sum_{k=1}^{d} \mathbf{a}_k s(t-\tau_k) e^{j\omega_{D_k} t} + \mathbf{n}(t) \tag{1}$$

where d represents the number of different multipath signals and where the parameters τ_k, ω_{D_k}, and $\mathbf{a}_k$ are the time delay, frequency offset, and spatial signature of the kth arrival. The additive noise vector $\mathbf{n}(t)$ is assumed to be a zero mean temporally and spatially white noise process with covariance $\sigma^2\mathbf{I}$. The standard narrowband assumption is employed here, i.e., the propagation time of the signal across the array is assumed to be much less than the reciprocal of the signal bandwidth. Note that for the radar case, the frequency offset ω_{D_k} is a narrowband approximation to the stretching or shrinking of the frequency axis due to the Doppler effect induced by the relative motion of the reflecting target.

The model in (1) could be further parameterized in terms of a set of DOA's. For example, if we let $\mathbf{a}(\theta)$ represent the array response to a unit amplitude plane wave arriving from the DOA θ, then $\mathbf{a}_k$ might be written as

$$\mathbf{a}_k = \sum_{i=1}^{d_k} \alpha_{ik} \mathbf{a}(\theta_{ik}) \tag{2}$$

where α_{ik} and θ_{ik} denote the complex amplitudes and DOA's associated with the ith arrival in the kth cluster of echos that have the same delay and Doppler shift. Here, to simplify the problem, we do not use this explicit parameterization of the spatial response in terms of DOA's but instead treat the elements of $\mathbf{a}_k$ as deterministic parameters to be estimated. This allows us to consider a cluster of coherent arrivals that share a given time delay and Doppler shift without the necessity of estimating the number of such arrivals nor their individual DOA's and amplitudes. After an estimate $\hat{\mathbf{a}}_k$ is obtained, d_k, α_{ik}, and θ_{ik} could be estimated, if desired, by using a least-squares fit of the model in (2).

Assuming that $\mathbf{x}(t)$ is an $m \times 1$ column vector and that a total of N snapshots are collected from the array, the data may be arranged in matrix form as

$$\begin{aligned} \mathbf{X}_t &\triangleq \begin{bmatrix} \mathbf{x}^T(t_1) \\ \vdots \\ \mathbf{x}^T(t_N) \end{bmatrix} \\ &= (\mathbf{S}_t(\boldsymbol{\tau}) \odot \mathbf{V}_t(\boldsymbol{\omega}))\mathbf{A} + \mathbf{N}_t \qquad (3) \\ &\triangleq \mathbf{Q}_t(\boldsymbol{\tau}, \boldsymbol{\omega})\mathbf{A} + \mathbf{N}_t \qquad (4) \end{aligned}$$

where $\mathbf{N}_t$ is formed in the same way as $\mathbf{X}_t$, $\odot$ denotes the Schur–Hadamard product, and

$$\begin{aligned} \boldsymbol{\tau} &= [\tau_1 \ \cdots \ \tau_d]^T \\ \boldsymbol{\omega} &= [\omega_{D_1} \ \cdots \ \omega_{D_d}]^T \\ \mathbf{A} &= [\mathbf{a}_1^T \ \cdots \ \mathbf{a}_d^T]^T \\ \mathbf{S}_t(\boldsymbol{\tau}) &= [\mathbf{s}_t(\tau_1) \ \cdots \ \mathbf{s}_t(\tau_d)] \\ \mathbf{s}_t(\tau) &= [s(t_1-\tau) \ \cdots \ s(t_N-\tau)]^T \\ \mathbf{V}_t(\boldsymbol{\omega}) &= [\mathbf{v}_t(\omega_{D_1}) \ \cdots \ \mathbf{v}_t(\omega_{D_d})] \\ \mathbf{v}_t(\omega) &= [e^{j\omega t_1} \ \cdots \ e^{j\omega t_N}]^T. \end{aligned}$$

The columns of the matrix $\mathbf{Q}_t(\boldsymbol{\tau}, \boldsymbol{\omega})$ are given by

$$\mathbf{q}_t(\tau_k, \omega_{D_k}) = \mathbf{s}_t(\tau_k) \odot \mathbf{v}_t(\omega_{D_k}).$$

The subscript t is used to distinguish the above time-domain model from its frequency domain counterpart presented below.

The frequency domain representation of the array output in (1) is given by

$$\mathbf{x}(\omega) = \sum_{k=1}^{d} \mathbf{a}_k s(\omega - \omega_{D_k}) e^{-j\omega\tau_k} + \mathbf{n}(\omega) \tag{5}$$

where $\mathbf{x}(\omega)$, $s(\omega)$, and $\mathbf{n}(\omega)$ are the Fourier transforms of $\mathbf{x}(t)$, $s(t)$, and $\mathbf{n}(t)$, respectively, and we have lumped the constant term $e^{j\omega_{D_k}\tau_k}$ together with $\mathbf{a}_k$. Under the assumption that the frequency/Doppler offsets are "small," it is possible to simplify the dependence of (5) on the Doppler frequencies

by neglecting the higher order terms in the Taylor series expansion of $s(\omega - \omega_{D_k})$

$$\begin{bmatrix} s(\omega_1 - \omega_{D_k}) \\ \vdots \\ s(\omega_N - \omega_{D_k}) \end{bmatrix} \approx \mathbf{s} - \omega_{D_k}\mathbf{d} \tag{6}$$

where

$$\mathbf{s} = [s(\omega_1) \ \cdots \ s(\omega_N)]^T$$
$$\mathbf{d} = [d(\omega_1) \ \cdots \ d(\omega_N)]^T$$
$$d(\omega_i) = \left.\frac{\partial s(\omega)}{\partial \omega}\right|_{\omega=\omega_i}.$$

As with $\mathbf{x}(t)$, we assume that $\mathbf{x}(\omega)$ is an $m \times 1$ column vector, and we collect the array data at frequencies $\omega_1, \cdots, \omega_N$ in matrix form as

$$\mathbf{X} \triangleq \begin{bmatrix} \mathbf{x}^T(\omega_1) \\ \vdots \\ \mathbf{x}^T(\omega_N) \end{bmatrix}$$
$$= (\mathbf{S}\mathbf{V}(\boldsymbol{\tau}) - \mathbf{D}\mathbf{V}(\boldsymbol{\tau})\boldsymbol{\Phi}(\boldsymbol{\omega}))\mathbf{A} + \mathbf{N} \tag{7}$$
$$\triangleq \mathbf{Q}(\boldsymbol{\tau}, \boldsymbol{\omega})\mathbf{A} + \mathbf{N} \tag{8}$$

where

$$\mathbf{S} = \text{diag}(\mathbf{s}) \tag{9}$$
$$\mathbf{D} = \text{diag}(\mathbf{d}) \tag{10}$$
$$\mathbf{V}(\boldsymbol{\tau}) = [\mathbf{v}(\tau_1) \ \cdots \ \mathbf{v}(\tau_d)] \tag{11}$$
$$\mathbf{v}(\tau) = [\exp(-j\omega_1\tau) \ \cdots \ \exp(-j\omega_N\tau)]^T \tag{12}$$
$$\boldsymbol{\Phi}(\boldsymbol{\omega}) = \text{diag}(\boldsymbol{\omega}) \tag{13}$$

and where, for example, $\text{diag}(\boldsymbol{\omega})$ is a diagonal matrix with the elements of the vector $\boldsymbol{\omega}$ along its diagonal. The columns of $\mathbf{Q}(\boldsymbol{\tau}, \boldsymbol{\omega})$ have the form

$$\mathbf{q}(\tau_k, \omega_{D_k}) = \mathbf{S}\mathbf{v}(\tau_k) - \omega_{D_k}\mathbf{D}\mathbf{v}(\tau_k). \tag{14}$$

In practice, $\mathbf{X}$ is obtained by performing a DFT on the time domain data in $\mathbf{X}_t$. As such, the translation of time delays into a linearly increasing phase shift $e^{-j\omega\tau}$ does not hold exactly, except in certain special cases involving, for example, a periodic signal or a signal with finite time support. However, if $t_N - t_1 \gg \max_k \tau_k$ and the signal is sampled at least at the Nyquist rate, then the error induced by the finite length DFT will be small, and the frequency domain model will be a reasonable approximation (this is illustrated by the simulation results in Section V). As explained below, the model in (8) has some interesting links with the well-known DOA estimation problem.

B. Connections with DOA Estimation

By interchanging the roles of the samples in time and space, the delay and Doppler estimation problem can be cast into the more familiar framework of DOA estimation. To see this, compare (8) with the standard model used in DOA estimation

$$\mathbf{X} = \mathbf{A}(\boldsymbol{\theta})\mathbf{S} + \mathbf{N} \tag{15}$$

where $\boldsymbol{\theta}$ is a vector containing the DOA's of the signals. In (15), $\mathbf{A}$ is a known function of the d parameters in $\boldsymbol{\theta}$, and $\mathbf{S}$ is usually treated as an unknown unstructured matrix. On the other hand, in (8), it is $\mathbf{Q}$ that is parameterized and $\mathbf{A}$ that is unstructured. In essence, the roles of time (frequency) and space have thus been reversed. Instead of the array manifold $\mathbf{a}(\theta)$ in m-space employed in the DOA model, the delay/Doppler model uses a "signal" manifold $\mathbf{q}(\tau_k, \omega_{D_k})$ in N-space.

A closer parallel may be drawn by comparing (8) with the generalized array manifold that is associated with polarized antenna arrays [4], [5] and signals with angular spread [6]. For dual polarized arrays, the array manifold is a combination of the response due to each polarization

$$\mathbf{A}(\boldsymbol{\theta}, \boldsymbol{\phi}_h, \boldsymbol{\phi}_v) = \mathbf{A}_h(\boldsymbol{\theta})\boldsymbol{\Phi}_h + \mathbf{A}_v(\boldsymbol{\theta})\boldsymbol{\Phi}_v \tag{16}$$

where $\mathbf{A}_h$, $\mathbf{A}_v$, and the diagonal matrices $\boldsymbol{\Phi}_h = \text{diag}(\boldsymbol{\phi}_h)$ and $\boldsymbol{\Phi}_v = \text{diag}(\boldsymbol{\phi}_v)$ represent the array response and the relative contribution of the horizontal and vertical polarization components, respectively. In the angular spread model of [6], the array manifold is given by

$$\mathbf{A}(\boldsymbol{\theta}, \boldsymbol{\phi}) = \mathbf{A}(\boldsymbol{\theta}) + \mathbf{D}(\boldsymbol{\theta})\boldsymbol{\Phi} \tag{17}$$

where the columns of $\mathbf{D}(\boldsymbol{\theta})$ are the derivatives of the columns of $\mathbf{A}(\boldsymbol{\theta})$ with respect to each element of $\boldsymbol{\theta}$, and $\boldsymbol{\Phi} = \text{diag}(\boldsymbol{\phi})$ is a $d \times d$ diagonal matrix whose elements $\boldsymbol{\phi}$ are a function of the DOA's and amplitudes of the local scatterers for each source. In [4]–[6], algorithms were developed that estimate the linear parameters (i.e., the elements of the diagonal matrices denoted by $\boldsymbol{\Phi}$ above) in closed-form and require only a search over the d elements of $\boldsymbol{\theta}$. In this paper, a similar approach is proposed for separating out the estimation of $\boldsymbol{\omega}$ from that of $\boldsymbol{\tau}$.

A classical approach to DOA estimation is the standard delay-and-sum beamformer, which maximizes

$$P(\theta) = \sum_{p=1}^{N} |\mathbf{a}^*(\theta)\mathbf{x}(t_p)|^2 \tag{18}$$

with respect to θ. Equation (18) can be thought of as a spatial matched filter. Similarly, the classical approach for time delay and Doppler estimation also involves a matched filter that correlates the received signal $\mathbf{x}(t)$ with a delayed and frequency shifted version of the known signal [7], [8]

$$\hat{\tau}, \hat{\omega}_D = \arg\max_{\tau, \omega_D} \left\| \sum_{p=1}^{N} s^*(t_p - \tau)e^{-j\omega_D t_p}\mathbf{x}(t_p) \right\|^2$$
$$= \arg\max_{\tau, \omega_D} \sum_{k=1}^{m} |\mathbf{q}_t^*(\tau, \omega_D)\mathbf{X}_{t,k}|^2 \tag{19}$$

where $\mathbf{X}_{t,k}$ denotes the kth column of $\mathbf{X}_t$. Both the classical beamforming method in (18) and the matched filtering approach of (19) are known to be optimal in the maximum likelihood sense if only a single signal is received ($d = 1$). However, neither (18) nor (19) is consistent when multiple arrivals are present. In Section III, we present several methods that overcome the drawbacks of (19) in the multiple echo case. These methods are counterparts to the subspace fitting

[5], [15]–[17], MUSIC [3], [4], and ESPRIT [14] algorithms developed for DOA estimation.

C. Identifiability

The parameters of the model in (4) are said to be identifiable if

$$\mathbf{Q}_t(\boldsymbol{\tau}, \boldsymbol{\omega})\mathbf{A} \neq \mathbf{Q}_t(\boldsymbol{\tau}', \boldsymbol{\omega}')\mathbf{A}' \tag{20}$$

whenever $\boldsymbol{\tau} \neq \boldsymbol{\tau}'$, $\boldsymbol{\omega} \neq \boldsymbol{\omega}'$, or $\mathbf{A} \neq \mathbf{A}'$. In other words, the unknown parameters $\boldsymbol{\tau}, \boldsymbol{\omega}$, and $\mathbf{A}$ should be uniquely determinable from noise-free data. We use the time-domain signal manifold here since it does not rely on any approximations, such as the one used in (6) for the frequency domain model. Because of the similarities between (4) and (15), the identifiability results of [18] for DOA estimation can be applied here. Our model employs a signal manifold $\mathbf{q}_t(\tau, \omega)$ in N-space instead of the array manifold $\mathbf{a}(\theta)$ in m-space. As with $\mathbf{a}(\theta)$, the signal's temporal signature $\mathbf{q}_t(\tau, \omega)$ is said to be *unambiguous* if every collection of N distinct vectors from the signal manifold is linearly independent. Reversing the role of time and space, we obtain the following theorem.

Theorem 1: Suppose an m-element array receives d delayed and frequency/Doppler-shifted copies of a known waveform. If the signal manifold is unambiguous, then the delays $\boldsymbol{\tau}$, the frequency shifts $\boldsymbol{\omega}$, and the spatial signatures in $\mathbf{A}$ can be uniquely determined, provided that

$$d < \frac{N + m'}{2} \tag{21}$$

where $m' = \text{rank}(\mathbf{A})$. If instead

$$d < \frac{m'}{m' + 1} N \tag{22}$$

then $\boldsymbol{\tau}$, $\boldsymbol{\omega}$, and $\mathbf{A}$ may be uniquely determined with probability one.

Proof: The proof is identical to that given in [18] for the case where there are two parameters per source (e.g., as in azimuth and elevation DOA estimation). ■

It is reasonable to assume that in most situations, the matrix $\mathbf{A}$ will be full rank so that $m' = \min(m, d)$. However, $\mathbf{A}$ may be ill-conditioned in situations where signals with different time delays or Doppler shifts arrive with nearly coincident DOA's. When $m' = d$, identifiability is guaranteed, provided that $d < N$. In the case when $m' = m$, the upper bound in (21) approaches $d < N/2$ for large N. In either case, the number of resolvable signal paths is only limited by the amount of data collected from the array.

The algorithms described in the next few sections use the approximate frequency domain model of (6)–(14) rather than the "exact" time domain model assumed in the discussion of identifiability above. As such, they require that an additional assumption be made in order to guarantee uniqueness. In particular, the algorithms require that there be no more than two signal clusters with different Doppler shifts that share the same delay. This results because of the linear dependence of the temporal signature on ω_{D_k} in (14). To see this, note that the vectors of $\mathbf{q}(\tau, \omega_1)$ and $\mathbf{q}(\tau, \omega_2)$ are linearly independent as long as $\omega_1 \neq \omega_2$. However, a third vector $\mathbf{q}(\tau, \omega_3)$ with the same delay can be written as a linear combination of $\mathbf{q}(\tau, \omega_1)$ and $\mathbf{q}(\tau, \omega_2)$, and thus, the three Doppler parameters could not be distinguished from one another using only $\mathbf{x}(\omega)$. As a practical matter, it is very difficult even to distinguish between two vectors $\mathbf{q}(\tau, \omega_1)$ and $\mathbf{q}(\tau, \omega_2)$ since ω_1 and ω_2 are so small. Note, however, that there is no problem handling the case where there are multiple arrivals with the same Doppler shift but different time delays.

III. Maximum Likelihood Estimation and the Cramér–Rao Lower Bound

Assuming temporally and spatially white circular Gaussian noise and treating $\mathbf{A}$ as an unstructured deterministic matrix, the ML solution is easily shown to be equivalent to the least-squares problem

$$\begin{aligned}\hat{\boldsymbol{\tau}}, \hat{\boldsymbol{\omega}}, \hat{\mathbf{A}} &= \arg \min_{\boldsymbol{\tau}, \boldsymbol{\omega}, \mathbf{A}} V_{\text{ML}}(\boldsymbol{\tau}, \boldsymbol{\omega}, \mathbf{A}) \\ &= \arg \min_{\boldsymbol{\tau}, \boldsymbol{\omega}, \mathbf{A}} \|\mathbf{X} - \mathbf{Q}(\boldsymbol{\tau}, \boldsymbol{\omega})\mathbf{A}\|_F^2 \end{aligned} \tag{23}$$

where $\|\cdot\|_F$ denotes the Frobenius norm. Note that (23) could be used with the time domain data $\mathbf{X}_t$ and manifold $\mathbf{Q}_t(\boldsymbol{\tau}, \boldsymbol{\omega})$ as well. The loss function in (23) can be explicitly minimized with respect to $\mathbf{A}$, which yields

$$\hat{\mathbf{A}} = \mathbf{Q}^{\dagger}(\hat{\boldsymbol{\tau}}, \hat{\boldsymbol{\omega}})\mathbf{X} \tag{24}$$

where

$$\begin{aligned}\hat{\boldsymbol{\tau}}, \hat{\boldsymbol{\omega}} &= \arg \min_{\boldsymbol{\tau}, \boldsymbol{\omega}} \|\boldsymbol{\Pi}^{\perp}_{\mathbf{Q}(\boldsymbol{\tau}, \boldsymbol{\omega})}\mathbf{X}\|_F^2 \\ &= \arg \max_{\boldsymbol{\tau}, \boldsymbol{\omega}} \text{tr}\{\mathbf{X}^* \boldsymbol{\Pi}_{\mathbf{Q}(\boldsymbol{\tau}, \boldsymbol{\omega})}\mathbf{X}\} \end{aligned} \tag{25}$$

and where $\text{tr}\{\cdot\}$ denotes the matrix trace, $(\cdot)^*$ the conjugate transpose, $(\cdot)^{\dagger}$ the pseudo inverse, and

$$\boldsymbol{\Pi}^{\perp}_{\mathbf{Q}(\boldsymbol{\tau}, \boldsymbol{\omega})} = \mathbf{I} - \boldsymbol{\Pi}_{\mathbf{Q}(\boldsymbol{\tau}, \boldsymbol{\omega})} = \mathbf{I} - \mathbf{Q}(\boldsymbol{\tau}, \boldsymbol{\omega})\mathbf{Q}^{\dagger}(\boldsymbol{\tau}, \boldsymbol{\omega})$$

is the orthogonal projection matrix onto the null space of $\mathbf{Q}^*(\boldsymbol{\tau}, \boldsymbol{\omega})$.

Unlike the (deterministic) ML estimator for the DOA problem, the ML estimates obtained from (24) and (25) will be consistent and asymptotically efficient, i.e., the estimates will asymptotically (as $N \to \infty$) achieve the Cramér–Rao lower bound (CRB). This results since $\mathbf{Q}^{\dagger}(\hat{\boldsymbol{\tau}}, \hat{\boldsymbol{\omega}})$ in (24) is orthogonal to the noise matrix $\mathbf{N}$ as $N \to \infty$. The asymptotic condition $N \to \infty$ for the delay/Doppler estimation problem considered here is similar to the DOA estimation problem studied in [19], where the number of sensors was assumed to be large. Details on the properties of the ML estimator for this latter case can be found therein.

Next, we present the CRB associated with the time-domain model (4). A similar CRB formula holds for the frequency domain model (8), but we focus on (4) here since it is the "exact" representation of our data. As a general rule, all estimators discussed in this paper are based on the approximate frequency domain model, but the data are generated by the "exact" time-domain equation, and accordingly, the CRB performance is evaluated for the latter model. The CRB is

given by the inverse of the Fisher information matrix (FIM) (see, e.g., [20, App. B]) as

$$\mathrm{FIM}_{k,p}(\boldsymbol{\xi}) = \frac{2}{\sigma^2}\sum_{t=1}^{N}\mathrm{Re}\left\{\frac{\partial \mu_t^*}{\partial \xi_k}\frac{\partial \mu_t}{\partial \xi_p}\right\} \tag{26}$$

where

$$\begin{aligned}\boldsymbol{\xi} &= [\boldsymbol{\omega}^T \quad \boldsymbol{\tau}^T \quad \boldsymbol{\gamma}_{\mathbf{A}}^R \quad \boldsymbol{\gamma}_{\mathbf{A}}^I]^T\\ \mu_t &= \mathbf{A}^T\boldsymbol{\nu}_s\\ \boldsymbol{\gamma}_{\mathbf{A}}^R &= (\mathrm{vec}[\mathrm{Re}\{\mathbf{A}\}])^T\\ \boldsymbol{\gamma}_{\mathbf{A}}^I &= (\mathrm{vec}[\mathrm{Im}\{\mathbf{A}\}])^T\\ \boldsymbol{\nu}_s &= \begin{bmatrix} s(t-\tau_1)e^{j\omega_{D_1}t}\\ \vdots\\ s(t-\tau_d)e^{j\omega_{D_d}t}\end{bmatrix}\end{aligned}$$

and $\mathrm{Re}\{\mathbf{A}\}$ and $\mathrm{Im}\{\mathbf{A}\}$ denote the real and imaginary parts of the spatial signature matrix $\mathbf{A}$ and where $\mathrm{vec}(\cdot)$ is the vectorization operator.

For the case where ξ_i is a time delay or Doppler shift, the partial derivatives required to evaluate (26) can be written as

$$\frac{\partial \mu_t}{\partial \tau_i} = -\mathbf{a}_i^T\, d(t-\tau_i)e^{j\omega_{D_i}t} \tag{27}$$

$$\frac{\partial \mu_t}{\partial \omega_{D_i}} = \mathbf{a}_i^T\, jts(t-\tau_i)e^{j\omega_{D_i}t} \tag{28}$$

where

$$d(t) = \frac{\partial s(t)}{\partial t}. \tag{29}$$

The partial derivatives with respect to the real and imaginary parts of the k,pth element of $\mathbf{A}$ can also be easily found.

In general, finding the ML estimates of $\boldsymbol{\tau}$ and $\boldsymbol{\omega}$ from (25) requires a multidimensional search over a $2d$-dimensional parameter space, which may be computationally burdensome. In the next section, we present a number of subspace-based methods that estimate the parameters of interest in a more computationally efficient manner. Some of these methods have accuracy comparable with that of the ML approach (and the CRB).

IV. Subspace-Based Estimation Methods

In this section, we describe algorithms for time delay and frequency/Doppler offset estimation based on noise subspace fitting (NSF) [15], [17], signal subspace fitting (SSF) [15]–[17], MUSIC [3], and ESPRIT [14]. It will be shown that due to the special structure of the signal manifold in the frequency domain, both NSF and SSF reduce to a d-dimensional search for the delay parameters. Of the two, SSF is expected to be more robust when the spatial signature matrix $\mathbf{A}$ is nearly rank-deficient or when the time-delay differences are very small [17]. Both methods require initial estimates of the $\boldsymbol{\tau}$ parameters, and for this purpose, the MUSIC estimator and an ESPRIT-based estimator are derived. The MUSIC estimator requires d one-dimensional (1-D) searches, whereas the ESPRIT estimator, which ignores the Doppler shifts, does not require any search.

A. Noise Subspace Fitting

The NSF loss function for the problem at hand may be written as [5], [15]

$$\mathbf{V}_{\mathrm{NSF}}(\boldsymbol{\tau},\boldsymbol{\omega}) = \mathrm{tr}\{\mathbf{Q}^*(\boldsymbol{\tau},\boldsymbol{\omega})\hat{\mathbf{E}}_n\hat{\mathbf{E}}_n^*\mathbf{Q}(\boldsymbol{\tau},\boldsymbol{\omega})\hat{\mathbf{U}}\} \tag{30}$$

where

$$\hat{\mathbf{U}} = \mathbf{Q}^\dagger(\hat{\boldsymbol{\tau}},\hat{\boldsymbol{\omega}})\hat{\mathbf{E}}_s\mathbf{W}\hat{\mathbf{E}}_s^*\mathbf{Q}^{\dagger *}(\hat{\boldsymbol{\tau}},\hat{\boldsymbol{\omega}}) \tag{31}$$

$\hat{\boldsymbol{\tau}}$ and $\hat{\boldsymbol{\omega}}$ are consistent (initial) estimates of $\boldsymbol{\tau}$ and $\boldsymbol{\omega}$, $\mathbf{W}$ is a diagonal weighting matrix, $\hat{\mathbf{E}}_s$ is the matrix whose columns are the left singular vectors corresponding to the d largest singular values of $\mathbf{X}$, and $\hat{\mathbf{E}}_n$ is a $N\times(N-d)$ matrix whose columns are orthogonal to those of $\hat{\mathbf{E}}_s$. The choice of the matrix $\mathbf{W}$ depends on whether it is desired to approximate the so-called deterministic or stochastic ML solution (see [15] and [17] for details). In the simulations presented later, we use the stochastic ML weighting

$$\mathbf{W} = (\hat{\boldsymbol{\Lambda}}_s - \hat{\sigma}^2\mathbf{I})^2\hat{\boldsymbol{\Lambda}}_s^{-1} \tag{32}$$

where $\hat{\boldsymbol{\Lambda}}_s$ is a diagonal matrix formed from the d largest squared singular values of $\mathbf{X}$, and $\hat{\sigma}^2$ is a consistent estimate of the noise variance (obtained, for example, as the average of the $m-d$ smallest squared singular values of $\mathbf{X}$).

Introduce $\mathbf{P} = \hat{\mathbf{E}}_n\hat{\mathbf{E}}_n^*$, and write $\mathbf{Q}(\boldsymbol{\tau},\boldsymbol{\omega}) = \mathbf{SV} - \mathbf{DV\Phi}$ by eliminating the explicit dependency on $\boldsymbol{\tau}$ and $\boldsymbol{\omega}$ so that (30) becomes

$$\begin{aligned}\mathrm{tr}\{\mathbf{Q}^*\mathbf{PQ}\hat{\mathbf{U}}\} = &\mathrm{tr}\{\mathbf{V}^*\mathbf{S}^*\mathbf{PSV}\hat{\mathbf{U}}\}\\ &-\mathrm{tr}\{\mathbf{V}^*\mathbf{S}^*\mathbf{PDV\Phi}\hat{\mathbf{U}}\}\\ &-\mathrm{tr}\{\mathbf{\Phi}^*\mathbf{V}^*\mathbf{D}^*\mathbf{PSV}\hat{\mathbf{U}}\}\\ &+\mathrm{tr}\{\mathbf{\Phi}^*\mathbf{V}^*\mathbf{D}^*\mathbf{PDV\Phi}\hat{\mathbf{U}}\}.\end{aligned} \tag{33}$$

It is easily shown that

$$\mathrm{tr}\{\mathbf{Y}^*\mathbf{ZYF}\} = \mathbf{y}^*(\mathbf{Z}\odot\mathbf{F}^T)\mathbf{y} \tag{34}$$

where $\mathbf{Z}$ and $\mathbf{F}$ are arbitrary square matrices, and $\mathbf{Y} = \mathrm{diag}(\mathbf{y})$ is a diagonal matrix. Using (33) and (34), the NSF criterion in (30) can be rewritten as

$$\begin{aligned}\mathbf{V}_{\mathrm{NSF}}(\boldsymbol{\tau},\boldsymbol{\omega}) &= \boldsymbol{\eta}^T(\boldsymbol{\omega})\mathbf{M}(\boldsymbol{\tau})\boldsymbol{\eta}(\boldsymbol{\omega})\\ &= \boldsymbol{\eta}^T(\boldsymbol{\omega})\,\mathrm{Re}[\mathbf{M}(\boldsymbol{\tau})]\boldsymbol{\eta}(\boldsymbol{\omega})\end{aligned} \tag{35}$$

where

$$\begin{aligned}\boldsymbol{\eta}(\boldsymbol{\omega}) &= \begin{bmatrix}\boldsymbol{\omega}\\ \mathbf{e}\end{bmatrix}\\ \mathbf{M}(\boldsymbol{\tau}) &= \begin{bmatrix}(\mathbf{V}^*\mathbf{D}^*\mathbf{PDV}) & -(\mathbf{V}^*\mathbf{D}^*\mathbf{PSV})\\ -(\mathbf{V}^*\mathbf{S}^*\mathbf{PDV}) & (\mathbf{V}^*\mathbf{S}^*\mathbf{PSV})\end{bmatrix}\\ &\quad\odot\begin{bmatrix}\hat{\mathbf{U}}^T & \hat{\mathbf{U}}^T\\ \hat{\mathbf{U}}^T & \hat{\mathbf{U}}^T\end{bmatrix}\end{aligned} \tag{36}$$

and $\mathbf{e} = [1\ \cdots\ 1]^T$ is $d\times 1$.

Since the NSF criterion is quadratic in $\boldsymbol{\omega}$, the estimation of $\boldsymbol{\omega}$ is separable from that of $\boldsymbol{\tau}$. Setting $\partial\mathbf{V}_{\mathrm{NSF}}/\partial\boldsymbol{\omega} = \mathbf{0}$ yields

$$\hat{\boldsymbol{\omega}} = [\mathrm{Re}(\mathbf{M}_{11})]^{-1}\,\mathrm{Re}(\mathbf{M}_{12})\mathbf{e} \tag{37}$$

where the matrix $\mathbf{M}(\boldsymbol{\tau})$ has been partitioned into $d \times d$ blocks

$$\mathrm{Re}\,\mathbf{M}(\boldsymbol{\tau}) = \begin{bmatrix} \mathbf{M}_{11} & -\mathbf{M}_{12} \\ -\mathbf{M}_{21} & \mathbf{M}_{22} \end{bmatrix}.$$

Substituting (37) into (35) leads to the following criterion for estimating $\boldsymbol{\tau}$

$$\begin{aligned} \hat{\boldsymbol{\tau}} &= \arg\min_{\boldsymbol{\tau}} \boldsymbol{\eta}^T(\hat{\boldsymbol{\omega}})\mathbf{M}(\boldsymbol{\tau})\boldsymbol{\eta}(\hat{\boldsymbol{\omega}}) \\ &= \arg\min_{\boldsymbol{\tau}} \mathbf{e}^T(\mathbf{M}_{22} - \mathbf{M}_{12}^T\mathbf{M}_{11}^{-1}\mathbf{M}_{12})\mathbf{e} \end{aligned} \tag{38}$$

which is the sum of the elements of the Schur complement of $\mathrm{Re}(\mathbf{M}_{11})$ in $\mathrm{Re}(\mathbf{M}(\boldsymbol{\tau}))$.

It is worth mentioning that since, typically, $N \gg d$, it is advantageous to compute $\mathbf{P}$ as $\mathbf{P} = \mathbf{I} - \hat{\mathbf{E}}_s\hat{\mathbf{E}}_s^*$ rather than $\mathbf{P} = \hat{\mathbf{E}}_n\hat{\mathbf{E}}_n^*$. The computation of $\hat{\mathbf{E}}_s$ is cheaper than that of $\hat{\mathbf{E}}_n$. Additionally, calculation of the submatrices of $\mathbf{M}$ can be simplified if the required matrix products are performed in a certain order. For example, if we first compute the terms below in the parentheses

$$\mathbf{V}^*\mathbf{D}^*\mathbf{P}\mathbf{D}\mathbf{V} = (\mathbf{V}^*\mathbf{D}^*)(\mathbf{D}\mathbf{V}) - (\mathbf{V}^*\mathbf{D}^*\hat{\mathbf{E}}_s)(\hat{\mathbf{E}}_s^*\mathbf{D}\mathbf{V})$$

the required computation is of order $O(Nd^2)$ instead of $O(N^2d)$.

The NSF algorithm is implemented by performing a d-dimensional search of the criterion in (38). As mentioned above, consistent initial estimates of $\boldsymbol{\tau}$ and $\boldsymbol{\omega}$ are required to compute the matrix $\hat{\mathbf{U}}$ used in the NSF criterion. One way of obtaining $\hat{\mathbf{U}}$ would be to first implement the NSF algorithm with $\hat{\mathbf{U}} = \mathbf{I}$ and use the resulting estimates to form the optimal $\hat{\mathbf{U}}$. Setting $\hat{\mathbf{U}} = \mathbf{I}$ is equivalent to using the MUSIC approach described later in this section. There are two drawbacks associated with the NSF algorithm: First, the algorithm is not always able to resolve closely spaced components in $\boldsymbol{\tau}$, and second, the algorithm's performance may deteriorate when the rows of $\mathbf{A}$ are linearly dependent, which can occur when either $d > m$ or two arrivals with different delays share the same spatial signature. The SSF algorithm presented in the next section overcomes these two drawbacks.

B. Signal Subspace Fitting

The SSF estimates of the delays and frequency/Doppler offsets can be found by minimizing [15]–[17]

$$\mathbf{V}_{\mathrm{SSF}}(\boldsymbol{\tau}, \boldsymbol{\omega}) = \mathrm{tr}\{\boldsymbol{\Pi}_{\mathbf{Q}}^{\perp}\hat{\mathbf{E}}_s\mathbf{W}\hat{\mathbf{E}}_s^*\} \tag{39}$$

where the diagonal weighting $\mathbf{W}$ is as defined in (32). As shown below, the Doppler parameters can also be explicitly estimated using SSF but only for the case where $d < N/2$, which is not a serious restriction in most cases (see the discussion on identifiability in Section II-C).

Define

$$\mathbf{C} = [\mathbf{S}\mathbf{V} \;\; -\mathbf{D}\mathbf{V}] \tag{40}$$

and suppose that $d < N/2$ and $\mathbf{C}$ has full column rank. Let $\mathbf{B}$ be an $N \times (N-2d)$ matrix that spans the space orthogonal to the columns of $\mathbf{C}$ ($\mathbf{B}$ is used as a dummy variable in what follows), and define the $(N-d) \times N$ matrix $\mathbf{H}^*$ as

$$\mathbf{H}^* = \begin{bmatrix} \mathbf{B}^* \\ [\boldsymbol{\Phi} \;\; -\mathbf{I}]\mathbf{C}^{\dagger} \end{bmatrix}. \tag{41}$$

Observe that

$$\mathbf{H}^*\mathbf{Q} = \mathbf{H}^*\mathbf{C}\begin{bmatrix} \mathbf{I} \\ \boldsymbol{\Phi} \end{bmatrix} = \mathbf{0}$$

and that

$$\mathbf{H}^*\mathbf{H} = \begin{bmatrix} \mathbf{B}^*\mathbf{B} & 0 \\ 0 & [\boldsymbol{\Phi} \;\; -\mathbf{I}](\mathbf{C}^*\mathbf{C})^{-1}\begin{bmatrix} \boldsymbol{\Phi}^* \\ -\mathbf{I} \end{bmatrix} \end{bmatrix}$$

is nonsingular. Thus, the columns of $\mathbf{H}$ span the nullspace of $\mathbf{Q}^*$, and the projection matrix $\boldsymbol{\Pi}_{\mathbf{Q}}^{\perp}$ can be written as

$$\begin{aligned} \boldsymbol{\Pi}_{\mathbf{Q}}^{\perp} &= \boldsymbol{\Pi}_{\mathbf{H}} = \mathbf{H}\mathbf{H}^{\dagger} \\ &= \mathbf{I} - \mathbf{C}\mathbf{C}^{\dagger} + \mathbf{C}^{\dagger *}\begin{bmatrix} \boldsymbol{\Phi}^* \\ -\mathbf{I} \end{bmatrix}\mathbf{T}[\boldsymbol{\Phi} \;\; -\mathbf{I}]\mathbf{C}^{\dagger} \end{aligned}$$

where

$$\mathbf{T}^{-1} = [\boldsymbol{\Phi} \;\; -\mathbf{I}](\mathbf{C}^*\mathbf{C})^{-1}\begin{bmatrix} \boldsymbol{\Phi}^* \\ -\mathbf{I} \end{bmatrix}. \tag{42}$$

To make the SSF criterion quadratic in $\boldsymbol{\Phi}$, we assume that $\mathbf{T}$ is calculated using some initial consistent estimate of the parameters. With the resulting matrix $\hat{\mathbf{T}}$, we rewrite (39) approximately as

$$\mathbf{V}_{\mathrm{SSF}} = \mathrm{tr}\{(\mathbf{I} - \mathbf{C}\mathbf{C}^{\dagger})\hat{\mathbf{E}}_s\mathbf{W}\hat{\mathbf{E}}_s^*\} + \mathrm{tr}\{\boldsymbol{\Psi}\hat{\mathbf{T}}\} \tag{43}$$

where

$$\boldsymbol{\Psi} = \boldsymbol{\Phi}\boldsymbol{\Gamma}_{11}\boldsymbol{\Phi}^* - \boldsymbol{\Gamma}_{12}^*\boldsymbol{\Phi}^* - \boldsymbol{\Phi}\boldsymbol{\Gamma}_{12} + \boldsymbol{\Gamma}_{22} \tag{44}$$

and $\boldsymbol{\Gamma}_{ij}$ are the $d \times d$ blocks of the matrix

$$\boldsymbol{\Gamma} = \begin{bmatrix} \boldsymbol{\Gamma}_{11} & \boldsymbol{\Gamma}_{12} \\ \boldsymbol{\Gamma}_{12}^* & \boldsymbol{\Gamma}_{22} \end{bmatrix} \triangleq \mathbf{C}^{\dagger}\hat{\mathbf{E}}_s\mathbf{W}\hat{\mathbf{E}}_s^*\mathbf{C}^{\dagger *}. \tag{45}$$

Replacing $\mathbf{T}$ by the consistent estimate $\hat{\mathbf{T}}$ does not affect the asymptotic performance of the algorithm since

$$[\boldsymbol{\Phi} \;\; -\mathbf{I}]\mathbf{C}^{\dagger}\hat{\mathbf{E}}_s = o(1)$$

at the true values of $\boldsymbol{\tau}$ and $\boldsymbol{\omega}$.

Introducing $\boldsymbol{\alpha}$ as the vector formed from the real part of the diagonal elements of $\boldsymbol{\Gamma}_{12}\hat{\mathbf{T}}$, defining

$$\boldsymbol{\Omega} = \mathrm{Re}(\hat{\mathbf{T}} \odot \boldsymbol{\Gamma}_{11}^T) \tag{46}$$

$$\rho = \mathrm{tr}\{\boldsymbol{\Gamma}_{22}\hat{\mathbf{T}}\} \tag{47}$$

and using (34) once again, the part of the cost function that depends on the Doppler shifts can be written as

$$\begin{aligned} \mathrm{tr}\{\boldsymbol{\Psi}\hat{\mathbf{T}}\} &= \boldsymbol{\omega}^*\boldsymbol{\Omega}\boldsymbol{\omega} - \boldsymbol{\alpha}^*\boldsymbol{\omega} - \boldsymbol{\omega}^*\boldsymbol{\alpha} + \rho \\ &= \boldsymbol{\omega}^T\boldsymbol{\Omega}\boldsymbol{\omega} - 2\boldsymbol{\omega}^T\boldsymbol{\alpha} + \rho. \end{aligned} \tag{48}$$

Minimization of (48) with respect to $\boldsymbol{\omega}$ yields the estimate

$$\hat{\boldsymbol{\omega}} = \boldsymbol{\Omega}^{-1}\boldsymbol{\alpha}. \tag{49}$$

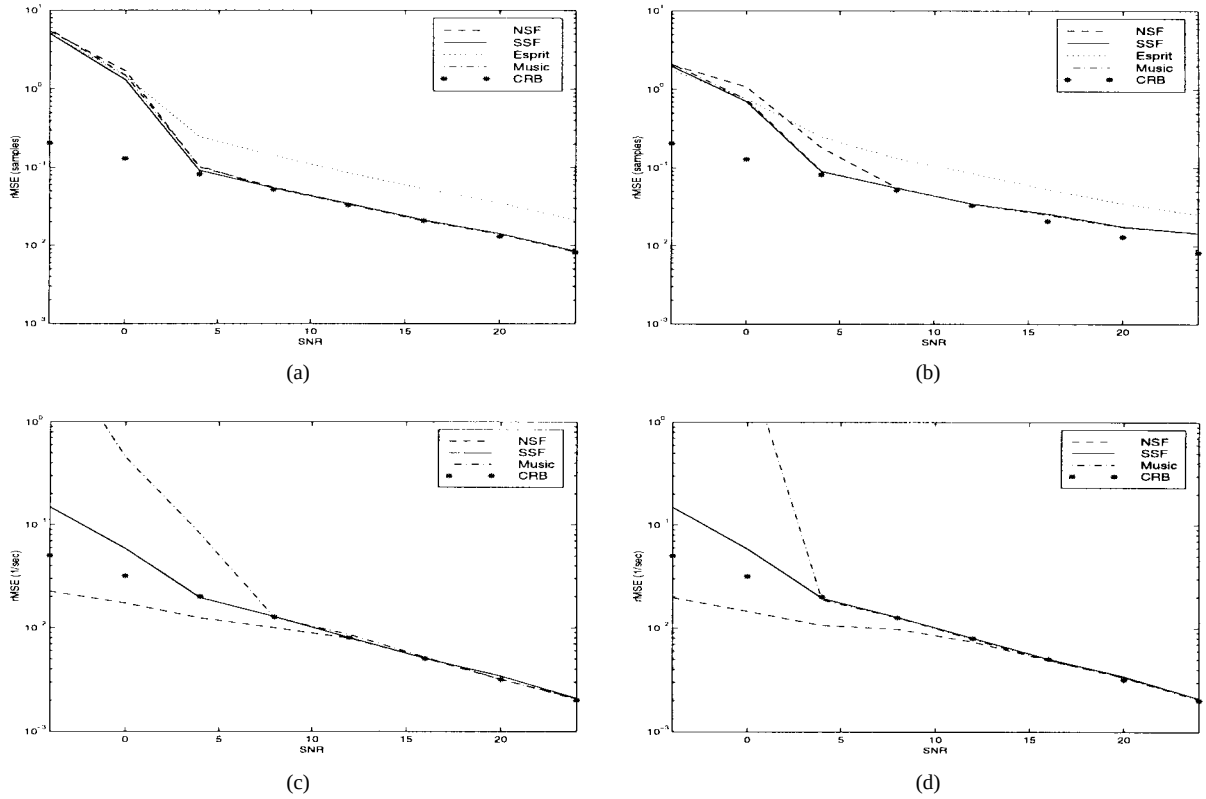

Fig. 1. rMSE of the proposed estimators as a function of the SNR compared with the corresponding CRB. (a) Time-delay τ_1. (b) Time-delay τ_2. (c) Doppler shift ω_1. (d) Doppler shift ω_2.

Inserting (49) into (43) leads to the estimate of $\boldsymbol{\tau}$ as

$$\hat{\boldsymbol{\tau}} = \arg\min_{\boldsymbol{\tau}} \rho - \boldsymbol{\alpha}^T \boldsymbol{\Omega}^{-1} \boldsymbol{\alpha} - \mathrm{tr}\{\mathbf{C}\mathbf{C}^{\dagger}\hat{\mathbf{E}}_s \mathbf{W} \hat{\mathbf{E}}_s^*\}. \tag{50}$$

Note that the computation required to evaluate the SSF criterion can be significantly simplified by performing the trace calculation in (50) as

$$\mathrm{tr}\{\mathbf{C}\mathbf{C}^{\dagger}\hat{\mathbf{E}}_s \mathbf{W} \hat{\mathbf{E}}_s^*\} = \mathrm{tr}\{(\mathbf{C}^{\dagger}\hat{\mathbf{E}}_s)\mathbf{W}(\hat{\mathbf{E}}_s^*\mathbf{C})\}.$$

The SSF algorithm is implemented by performing the d-dimensional search in (50). As with NSF, the SSF method requires consistent initial estimates of both $\boldsymbol{\tau}$ and $\boldsymbol{\omega}$ to form $\hat{\mathbf{T}}$, which is then used in calculating $\boldsymbol{\Omega}$ and $\boldsymbol{\alpha}$. Such estimates can be obtained using either the MUSIC or ESPRIT approaches presented in the following subsections or by an initial application of SSF with $\hat{\mathbf{T}} = \mathbf{I}$. It will be seen in Section V that as predicted, SSF outperforms NSF in cases where elements of $\boldsymbol{\tau}$ are closely spaced or when $\mathrm{rank}(\mathbf{A}) < d$ or nearly so. However, the algorithms perform almost identically at high SNR's.

C. MUSIC

In the standard MUSIC algorithm [3] for DOA estimation, the DOA's are determined to be the d values of θ that make $\mathbf{a}(\theta)$ nearly orthogonal to $\hat{\mathbf{E}}_n$, according to

$$\mathbf{V}_M(\theta) = \frac{\mathbf{a}^*(\theta)\hat{\mathbf{E}}_n\hat{\mathbf{E}}_n^*\mathbf{a}(\theta)}{\mathbf{a}^*(\theta)\mathbf{a}(\theta)}. \tag{51}$$

In the delay and Doppler estimation problem, assuming that $\mathrm{rank}(\mathbf{A}) = d$, we replace $\mathbf{a}(\theta)$ with the signal's frequency signature

$$\begin{aligned}\mathbf{q}(\tau, \omega_D) &= \mathbf{S}\mathbf{v}(\tau) - \omega_D \mathbf{D}\mathbf{v}(\tau) \\ &\triangleq \mathbf{G}(\tau)\mathbf{g}(\omega_D)\end{aligned} \tag{52}$$

where $\mathbf{g}(\omega) = [1 \ \omega_D]^T$, and

$$\mathbf{G}(\tau) = [\mathbf{S}\mathbf{v}(\tau) \quad -\mathbf{D}\mathbf{v}(\tau)].$$

For this case, the MUSIC loss function becomes

$$\mathbf{V}_M(\tau, \omega) = \frac{\mathbf{g}^*(\omega)[\mathrm{Re}(\mathbf{G}^*(\tau)\hat{\mathbf{E}}_n\hat{\mathbf{E}}_n^*\mathbf{G}(\tau))]\mathbf{g}(\omega)}{\mathbf{g}^*(\omega)[\mathrm{Re}(\mathbf{G}^*(\tau)\mathbf{G}(\tau))]\mathbf{g}(\omega)} \tag{53}$$

since $\mathbf{g}(\omega)$ is real valued. The MUSIC criterion in (53) is seen to be a ratio of quadratic forms in $\mathbf{g}(\omega)$, and thus, minimizing $\mathbf{V}_M(\tau, \omega)$ with respect to $\mathbf{g}(\omega)$ is equivalent to finding, as a function of τ, the minimum generalized eigenvalue and associated eigenvector of the following 2×2 matrices:

$$\mathrm{Re}(\mathbf{G}^*(\tau)\hat{\mathbf{E}}_n\hat{\mathbf{E}}_n^*\mathbf{G}(\tau))\boldsymbol{\gamma}_{\min} = \lambda_{\min}\,\mathrm{Re}(\mathbf{G}^*(\tau)\mathbf{G}(\tau))\boldsymbol{\gamma}_{\min}. \tag{54}$$

As in the algorithms of [3] and [4], the time delays can be found by viewing $\lambda_{\min}$ as a function of τ and searching for the d deepest minima of $\lambda_{\min}(\tau)$. The corresponding frequency offsets are then calculated using the generalized eigenvector associated with $\lambda_{\min}(\hat{\tau})$

$$\hat{\omega}_{D_k} = \frac{\boldsymbol{\gamma}_{\min,2}(\hat{\tau}_k)}{\boldsymbol{\gamma}_{\min,1}(\hat{\tau}_k)} \tag{55}$$

where $\boldsymbol{\gamma}_{\min,i}$ is element i of $\boldsymbol{\gamma}_{\min}$.

Note that the matrix $\mathbf{G}^*(\tau)\mathbf{G}(\tau)$ is actually independent of τ

$$\mathbf{G}^*(\tau)\mathbf{G}(\tau) = \begin{bmatrix} \|\mathbf{s}\|^2 & -\mathbf{s}^*\mathbf{d} \\ -\mathbf{d}^*\mathbf{s} & \|\mathbf{d}\|^2 \end{bmatrix}$$

which is a fact that simplifies evaluation of the above generalized MUSIC criterion. This observation also implies that the signal frequency sample vector $\mathbf{s}$ and the associated gradient vector $\mathbf{d}$ must be linearly independent for the algorithm to work.

D. ESPRIT

In [2], an algorithm based on ESPRIT was presented for estimating time delays in cases where the frequency/Doppler offset is zero. Our empirical results indicate that this approach still gives reasonable time delay estimates even when the frequency offset is nonzero but small. The fact that the algorithm yields the desired estimates in closed form (i.e., without a search) makes it an attractive alternative for initializing the SSF and NSF searches. The ESPRIT approach of [2] is briefly described below. Note that the algorithm is only applicable in cases where the rows of $\mathbf{A}$ are linearly independent (i.e., when rank$(\mathbf{A}) = d < m$).

Consider the frequency domain representation of (8) for the case with no frequency/Doppler offset

$$\mathbf{Q} = \mathbf{S}\mathbf{V}(\boldsymbol{\tau}). \tag{56}$$

Let $\mathbf{V}_1$ be the $(N-\delta)\times d$ matrix made from the first $N-\delta$ rows of $\mathbf{V}(\boldsymbol{\tau})$, and let $\mathbf{V}_2$ be constructed similarly from the last $N-\delta$ rows. If the data is evaluated at the DFT frequencies $\omega_k = 2\pi k/N$, $k = 1, \cdots, N$, then $\mathbf{V}(\boldsymbol{\tau})$ is Vandermonde, and its submatrices are related as

$$\mathbf{V}_2 = \mathbf{V}_1\boldsymbol{\Upsilon} \tag{57}$$

where

$$\boldsymbol{\Upsilon} = \begin{bmatrix} e^{-j2\pi\delta\tau_1/N} & & \\ & \ddots & \\ & & e^{-j2\pi\delta\tau_d/N} \end{bmatrix}. \tag{58}$$

Let $\mathbf{E}_s$ denote the noise-free left singular vectors of $\mathbf{X}$, and similarly define, for $\mathbf{E}_s$ and $\mathbf{S}$, the submatrices $\mathbf{E}_1$, $\mathbf{E}_2$, $\mathbf{S}_1$, and $\mathbf{S}_2$. Since, under the assumption that rank$(\mathbf{A}) = d$, the columns of $\mathbf{E}_s$ and $\mathbf{Q} = \mathbf{S}\mathbf{V}(\boldsymbol{\tau})$ span the same subspace, we have

$$\mathbf{E}_1 = \mathbf{S}_1\mathbf{V}_1\mathbf{T}_e \tag{59}$$

$$\mathbf{E}_2 = \mathbf{S}_2\mathbf{V}_2\mathbf{T}_e \tag{60}$$

for some $d\times d$ matrix $\mathbf{T}_e$. Combining (57)–(60) and eliminating $\mathbf{V}_1$ and $\mathbf{V}_2$ leads to

$$\mathbf{S}_1\mathbf{E}_2 = \mathbf{S}_2\mathbf{S}_1\mathbf{V}_1\boldsymbol{\Upsilon}\mathbf{T}_e = \mathbf{S}_2\mathbf{E}_1\mathbf{Z} \tag{61}$$

where $\mathbf{Z} = \mathbf{T}_e^{-1}\boldsymbol{\Upsilon}\mathbf{T}_e$.

Provided that δ is chosen small enough so that

$$\frac{N}{\delta} > \max_k \tau_k \tag{62}$$

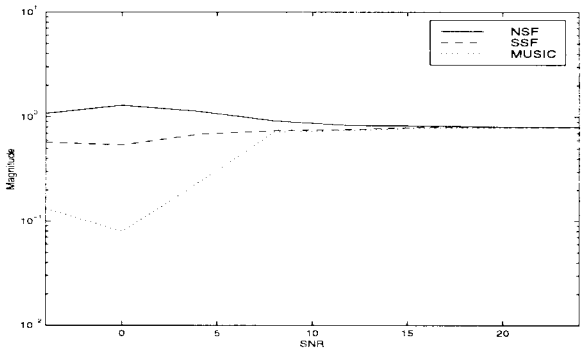

Fig. 2. Ratio of doppler estimate bias to standard deviation as a function of SNR.

there is a one-to-one relationship between the delays and the eigenvalues of $\mathbf{Z}$. With noisy data, $\mathbf{Z}$ must be estimated using $\hat{\mathbf{E}}_s$ and its submatrices $\hat{\mathbf{E}}_1$ and $\hat{\mathbf{E}}_2$. A simple least squares estimate of $\mathbf{Z}$ is given by

$$\hat{\mathbf{Z}} = (\mathbf{S}_2\hat{\mathbf{E}}_1)^\dagger\mathbf{S}_1\hat{\mathbf{E}}_2.$$

If $\hat{\lambda}_k$ denotes the kth eigenvalue of $\hat{\mathbf{Z}}$, the time delay estimates can be found from

$$\hat{\tau}_k = \frac{-N\arg\hat{\lambda}_k}{2\pi\delta}. \tag{63}$$

As shown in [2], [21], and [22], the variance of the ESPRIT estimates can be reduced by choosing the overlap factor δ to be as large as possible while still satisfying (62). In the simulations presented below, we use $\delta = 1$ for simplicity.

Although the above ESPRIT approach yields estimates of the time delays that are denoted by $\hat{\boldsymbol{\tau}}_e$, both NSF and SSF also require initial Doppler estimates to form the matrices $\hat{\mathbf{U}}$ and $\hat{\mathbf{T}}$. For NSF, an initial Doppler estimate can be obtained by substituting $\hat{\boldsymbol{\tau}}_e$ into (37) with either $\hat{\mathbf{U}} = \mathbf{I}$, or $\hat{\mathbf{U}}$ evaluated using $\hat{\boldsymbol{\tau}} = \hat{\boldsymbol{\tau}}_e$ and $\hat{\boldsymbol{\omega}} = 0$. Alternatively, for SSF, (49) can be used either with $\hat{\mathbf{T}} = \mathbf{I}$ or $\hat{\mathbf{T}}$ evaluated using $\hat{\boldsymbol{\tau}} = \hat{\boldsymbol{\tau}}_e$ and $\hat{\boldsymbol{\omega}} = 0$. A third approach would be to use MUSIC and the generalized eigenvector in (54) for every element of $\hat{\boldsymbol{\tau}}_e$ and then solve for the associated Doppler frequency using (55). All of these methods performed equally well in the numerical studies we have conducted. In the simulation results presented in Section V, the initial Doppler estimates for NSF and SSF were obtained using (37) with $\hat{\mathbf{U}} = \mathbf{I}$ and (49) with $\hat{\mathbf{T}} = \mathbf{I}$, respectively.

An ESPRIT solution similar to the one presented above can also be arrived at under a slightly different set of assumptions, without ignoring the Doppler component of the model. Using the notation developed above, but with the Doppler parameters included, the partitioned matrices of singular vectors will satisfy

$$\mathbf{E}_1 = (\mathbf{S}_1\mathbf{V}_1 - \mathbf{D}_1\mathbf{V}_1\boldsymbol{\Phi})\mathbf{T}_e \tag{64}$$

$$\mathbf{E}_2 = (\mathbf{S}_2\mathbf{V}_2 - \mathbf{D}_2\mathbf{V}_2\boldsymbol{\Phi})\mathbf{T}_e \tag{65}$$

where $\mathbf{D}_1$ and $\mathbf{D}_2$ are formed from $\mathbf{D}$ in the same way that $\mathbf{S}_1$ and $\mathbf{S}_2$ are formed from $\mathbf{S}$. Using (57), (65) may be rewritten as

$$\mathbf{E}_2 = (\mathbf{S}_2\mathbf{V}_1 - \mathbf{D}_2\mathbf{V}_1\boldsymbol{\Phi})\boldsymbol{\Upsilon}\mathbf{T}_e \tag{66}$$

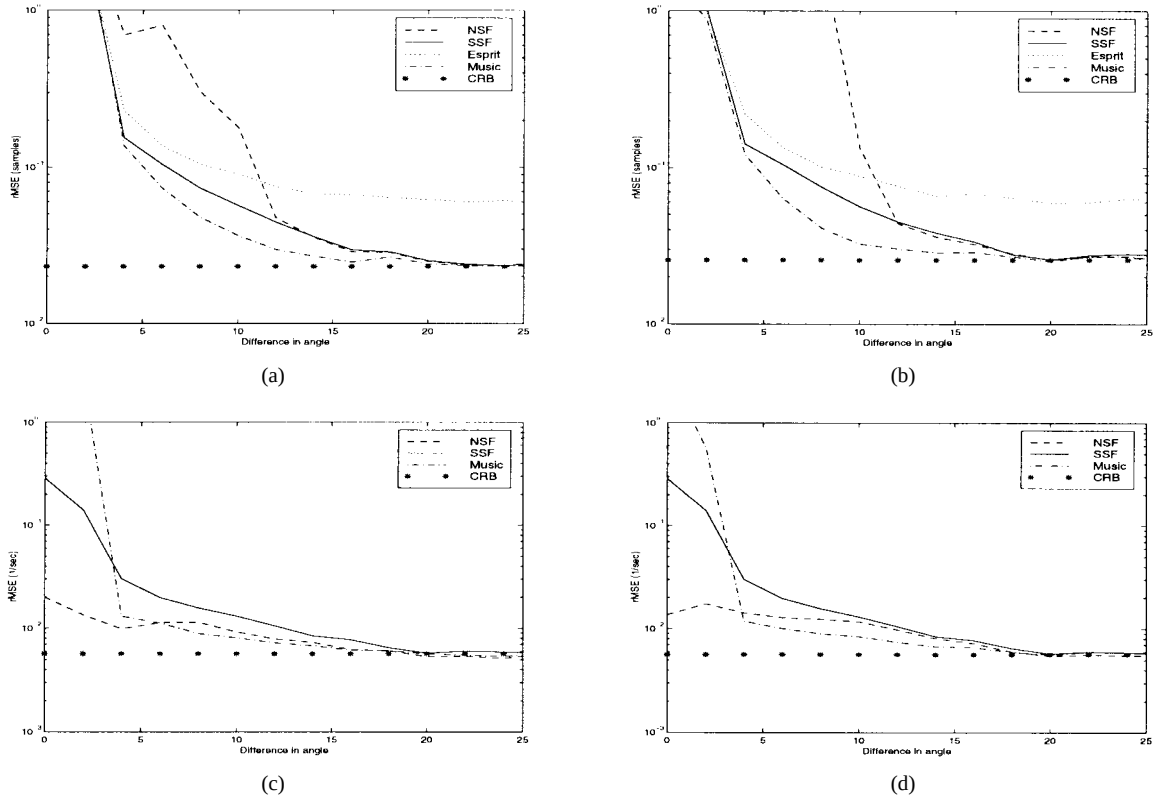

Fig. 3. rMSE of the proposed estimators as a function of the DOA difference compared with the corresponding CRB. (a) Time-delay τ_1. (b) Time-delay τ_2. (c) Doppler shift ω_1. (d) Doppler shift ω_2.

since the diagonal matrices $\mathbf{\Phi}$ and $\mathbf{\Upsilon}$ commute. Now, if it is assumed that the signal spectrum is smooth enough so that $\mathbf{S}_1 \simeq \mathbf{S}_2$ and $\mathbf{D}_1 \simeq \mathbf{D}_2$, then

$$\mathbf{E}_2 \simeq (\mathbf{S}_1\mathbf{V}_1 - \mathbf{D}_1\mathbf{V}_1\mathbf{\Phi})\mathbf{\Upsilon}\mathbf{T}_e \tag{67}$$

$$= \mathbf{E}_1\mathbf{T}_e^{-1}\mathbf{\Upsilon}\mathbf{T}_e \tag{68}$$

$$= \mathbf{E}_1\mathbf{Z} \tag{69}$$

and once again, the time delays can be found from the eigenvalues of $\mathbf{Z} = \mathbf{E}_1^{\dagger}\mathbf{E}_2$, which is equal to the matrix $\mathbf{Z}$ defined above for the case where $\mathbf{S}_1 = \mathbf{S}_2$. We note here that the smoothness condition $\mathbf{S}_1 \simeq \mathbf{S}_2$ was also used in [23] to find a simple ESPRIT time-delay solution for the case of zero Doppler.

V. Numerical Examples

A. Performance versus SNR

We begin by studying the performance of the algorithms presented above as the signal-to-noise ratio (SNR) varies. Simulation data was generated using (1) for two multipath signals ($d = 2$) with time delays $\boldsymbol{\tau} = [0.5\ 3]^T$ and Doppler shifts $\boldsymbol{\omega} = 2\pi[-0.02\ \ 0.01]^T$. The data was corrupted by spatially and temporally white circular Gaussian noise with zero mean and standard deviation σ. The two columns of the signature matrix $\mathbf{A}$ were given by the array response of a five-element, half-wavelength spaced, uniform linear array (ULA) to far-field sources with DOA's of 0 and 20°. The signal sequence was chosen to be

$$s(t) = \frac{\text{sinc}(t/T)}{1-(t/T)^2}.$$

For the simulations presented below, $T = 5$, and $N = 101$ samples are assumed to be taken from the array.

The root mean squared error (rMSE) of the time-delay and Doppler estimates were calculated for each of the algorithms based on 500 Monte Carlo trials for various SNR values. The results are plotted in Fig. 1, together with the appropriate CRB. The ESPRIT time-delay estimates (dotted line) were, as described in Section IV-D, used as the initial values for the NSF (dashed line) and the SSF (solid line) searches. Furthermore, the ESPRIT time-delay estimates were also used to initialize the local search for the MUSIC (dash-dotted line) time-delay estimates. As can be seen from the figures, all of the algorithms except ESPRIT achieve the CRB at about SNR $= 4$ dB. The excess error for the ESPRIT algorithm is, of course, due to the fact that it assumes the Doppler is zero when estimating the time delays; thus, it yields biased time delay estimates. The NSF and MUSIC algorithms failed to resolve the two signals in 10–20% of the trials below SNR $= 4$ dB (in which case, the two estimates were identical within numerical accuracy); when such a failure occurred, the single parameter value was assigned to be the estimate for both arrivals to compute the rMSE. It is interesting to note that the NSF Doppler estimates are actually below the CRB for low SNR's. This is due to the fact that the NSF Doppler estimates become biased in this region and approach zero as SNR $\rightarrow 0$. The excess bias for NSF is evident in Fig. 2, which plots

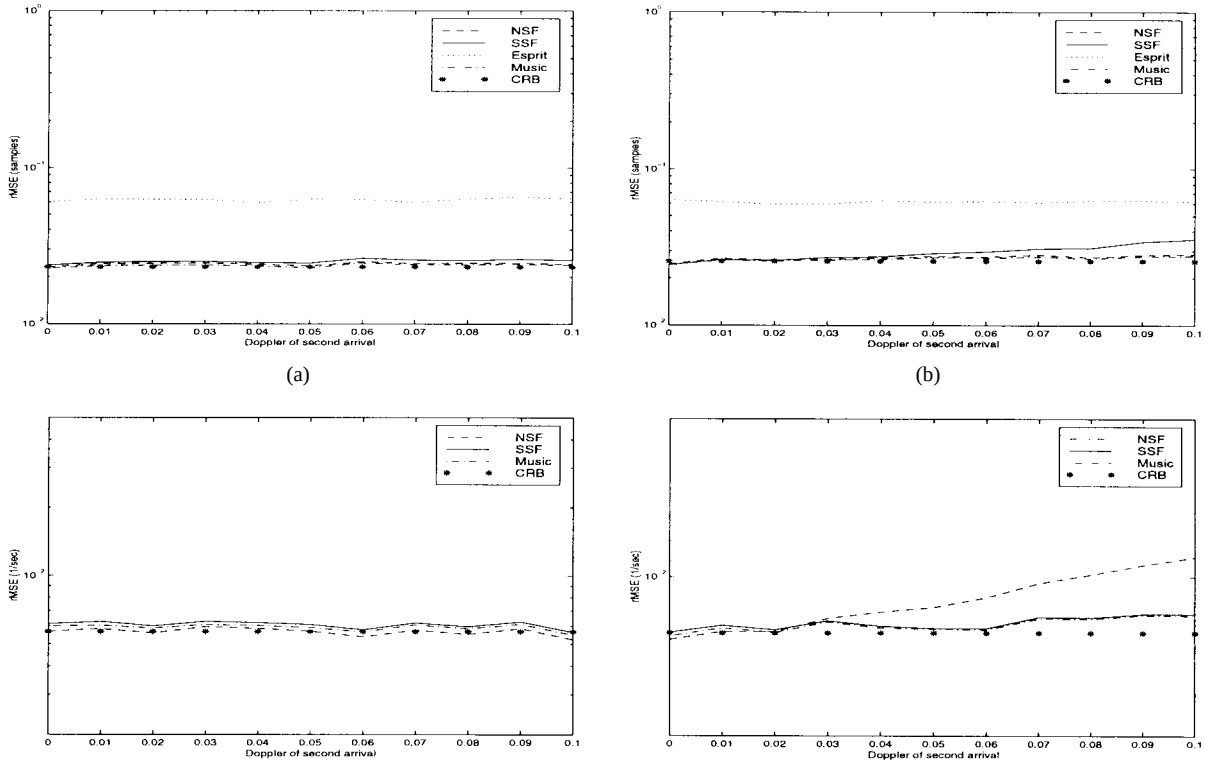

Fig. 4. rMSE of the proposed estimators as a function of the doppler shift difference compared with the corresponding CRB. (a) Time-delay τ_1. (b) Time-delay τ_2. (c) Doppler shift ω_1. (d) Doppler shift ω_2.

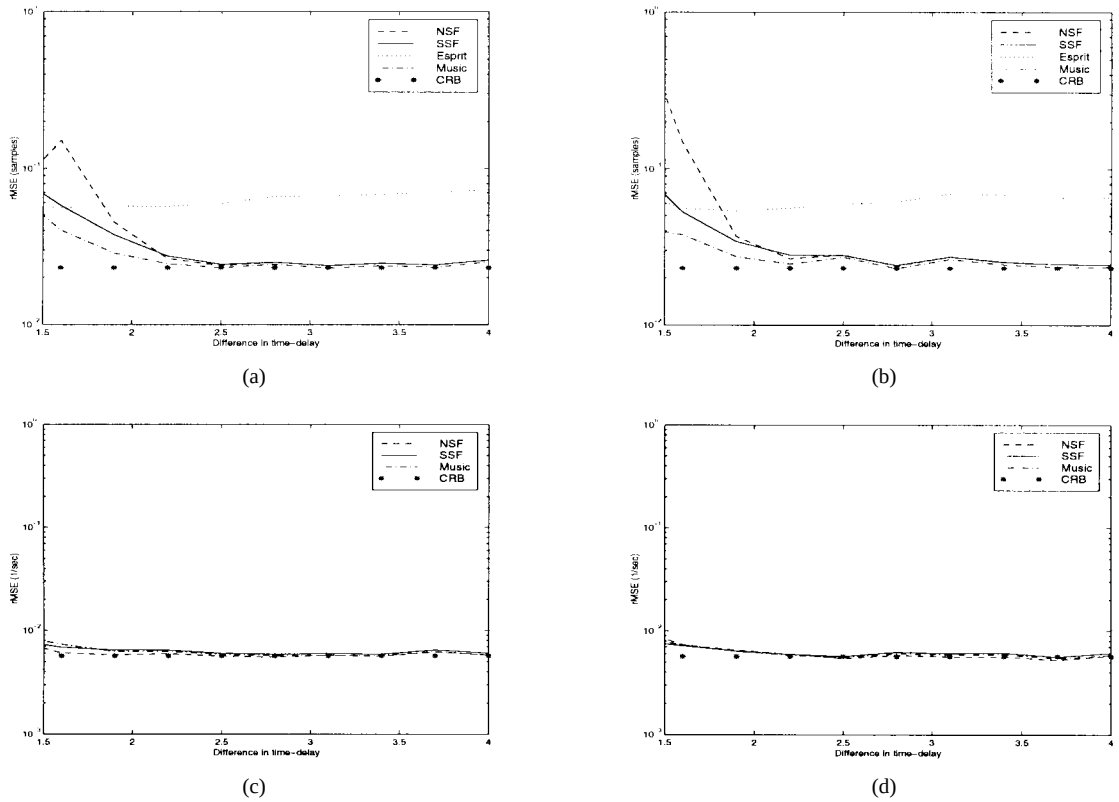

Fig. 5. rMSE of the proposed estimators as a function of the time–delay difference compared with the corresponding CRB. (a) Time-delay τ_1. (b) Time-delay τ_2. (c) Doppler shift ω_1. (d) Doppler shift ω_2.

the ratio of the bias and standard deviation of the Doppler estimate for the first arrival.

B. Closely Spaced Sources

Next, we study how the performance of the estimators depends on the assumption of a full rank spatial signature matrix. The data studied is as described above, but with SNR $= 15$ dB and DOA's $[0^\circ\ \theta]$, where the DOA of the second arrival θ is varied from 0 to 25°. Fig. 3(a) and (b) compare the estimation errors for the time-delay estimates, and as can be seen from the figures, the NSF, the SSF, and the MUSIC estimates achieve the CRB when the angular difference is above 15°. Furthermore, it is seen that all of the algorithms degrade significantly for angular differences lower than 5°. A nearly rank-deficient $\mathbf{A}$ matrix for our model corresponds to the coherent signal case in DOA estimation. Thus, we expect that MUSIC, NSF, and ESPRIT will all have poor performance in this case, and this is evident in the plots. SSF also degrades here due to the fact that it uses ESPRIT for initialization. Fig. 3(c) and (d) compare the rMSE for the Doppler shift estimates with the corresponding CRB. Here, the NSF and the MUSIC estimates are found to have a somewhat lower rMSE than the SSF estimates.

C. Large Doppler Shifts

In this case, we examine the robustness of the algorithms to the assumption that the Doppler shifts are small. We are reminded that the data are generated with (4), whereas all estimators use the model (8) obtained under the assumption of small Doppler offsets. The data studied is as described in Section V-A, but with SNR $= 15$ dB and with $\boldsymbol{\omega} = [-0.02\ \rho]$, where the Doppler shift of the second arrival ρ is varied from 0 to 0.1. Fig. 4(a) and (b) compare the estimation errors for the time-delay estimates with the corresponding CRB. Fig. 4(c) and (d) compare the Doppler shift estimation errors, and as can be seen from the figures, all the algorithms prove to be very robust to relatively large Doppler shifts.

D. Resolving Closely Spaced Arrivals

In our final example, we investigate the ability of the algorithms to resolve closely spaced arrivals. The case studied is as described previously in Section V-A, but with SNR $= 15$ 15 dB and with time delays $\boldsymbol{\tau} = [0.5\ 0.5 + \Delta]$, where the time-delay difference Δ is varied from 1.5 to 4. Fig. 5(a) and (b) compare the estimation errors for the time delays. As can be seen from the figures, the NSF, the SSF, and the MUSIC estimates achieve the CRB for a time-delay difference larger than 2. It was found that NSF was unable to resolve the two arrivals for $\Delta < 2$, whereas for MUSIC, the threshold was slightly better, as it lost resolution for $\Delta < 1.5$. Fig. 5(c) and (d) compare the estimation errors for the Doppler shifts. It is seen that for this case, the algorithms performances are not significantly affected by variations in the time-delay difference.

VI. Conclusions

In this paper, we have developed a data model for the time delay and Doppler shift estimation problem. We have illustrated the connection between the presented model and the polarization and angular spread models used in the DOA estimation case. Using the similarity between the models, we have developed general subspace-based time-delay and Doppler estimators. These estimators only require a search for the time-delay estimates since it is found that to first order, the subspace depends linearly on the Doppler parameters for small Doppler shifts. The performance of the algorithms was examined via several simulations, and it was found that the algorithms perform very well, even for large Doppler shifts well beyond those typically encountered in practice. For the cases considered, the SSF algorithm performed the best, and when it was able to resolve the sources, MUSIC had similar or, in some cases, even slightly better performance. On the other hand, the NSF algorithm had more trouble resolving arrivals for difficult cases. Although it was biased, ESPRIT was found to be an effective method for initializing the search-based methods.

References

[1] A. Swindlehurst, "Parametric synchronization and spatial signature estimation for multiple known co-channel signals," in *Proc. 29th Asilomar Conf. Signals, Syst., Comput.,* 1995.

[2] ———, "Time delay and spatial signature estimation using known asynchronous signals," *IEEE Trans. Signal Processing,* vol. 46, pp. 449–462, Feb. 1998.

[3] R. Schmidt, "A signal subspace approach to multiple emitter location and spectral estimation," Ph.D. thesis, Stanford Univ., Stanford, CA, 1981.

[4] E. R. Ferrara and T. M. Parks, "Direction finding with an array of antennas having diverse polarizations," *IEEE Trans. Antennas Propagat.,* vol. AP-31, pp. 231–236, Mar. 1983.

[5] A. Swindlehurst and M. Viberg, "Subspace fitting with diversely polarized antenna arrays," *IEEE Trans. Antennas Progapat.,* vol. 41, pp. 1687–1694, Dec. 1993.

[6] D. Asztély, B. Ottersten, and A. Swindlehurst, "A generalized array manifold model for local scattering in wireless communications," in *Proc. ICASSP,* Munich, Germany, 1997, pp. 4021–4024.

[7] H. L. Van Trees, *Detection, Estimation, and Modulation Theory, Part I.* New York: Wiley, 1968.

[8] C. Helstrom, *Elements of Signal Detection and Estimation.* Englewood Cliffs, NJ: Prentice-Hall, 1995.

[9] M. Wax, "The joint estimation of differential delay, Doppler, and phase," *IEEE Trans. Inform. Theory,* vol. IT-28, pp. 817–820, Sept. 1982.

[10] S. Stein, "Differential delay/Doppler estimation with unknown signals," *IEEE Trans. Signal Processing,* vol. 41, pp. 2717–2719, Aug. 1993.

[11] Q. Jin, K. Wong, and Z.-Q. Luo, "The estimation of time delay and Doppler stretch of wideband signals," *IEEE Trans. Signal Processing,* vol. 43, pp. 904–916, Apr. 1995.

[12] C. Couvreur and Y. Bresler, "Modeling and estimation for Doppler-shifted Gaussian random processes," in *Proc. 8th Workshop on Stat. Sig. and Array Proc.,* Corfu, Greece, June 1996, pp. 28–31.

[13] A. Habboosh, R. Vaccaro, and S. Kay, "An algorithm for detecting closely spaced delay/Doppler components," in *Proc. ICASSP,* Munich, Germany, 1997, pp. 535–538.

[14] R. Roy and T. Kailath, "ESPRIT—Estimation of signal parameters via rotational invariance techniques," *IEEE Trans. Acoust., Speech, Signal Processing,* vol. 37, pp. 984–995, July 1989.

[15] P. Stoica and K. Sharman, "Maximum likelihood methods for direction-of-arrival estimation," *IEEE Trans. Acoust., Speech, Signal Processing,* vol. 38, pp. 1132–1143, July 1990.

[16] M. Viberg and B. Ottersten, "Sensor array processing based on subspace fitting," *IEEE Trans. Signal Processing,* vol. 39, pp. 1110–1121, May 1991.

[17] B. Ottersten, M. Viberg, P. Stoica, and A. Nehorai, "Exact and large sample ML techniques for parameter estimation and detection in array

processing," in *Radar Array Processing*, Haykin, Litva, and Shepherd, Eds. Berlin, Germany: Springer-Verlag, 1993, pp. 99–151.
[18] M. Wax and I. Ziskind, "On unique localization of multiple sources by passive sensor arrays," *IEEE Trans. Acoust., Speech, Signal Processing*, vol. 37, pp. 996–1000, July 1989.
[19] M. Viberg, B. Ottersten, and A. Nehorai, "Performance analysis of direction finding with large arrays and finite data," *IEEE Trans. Signal Processing*, vol. 43, pp. 469–477, Feb. 1995.
[20] P. Stoica and R. Moses, *Introduction to Spectral Analysis.* Upper Saddle River, NJ: Prentice-Hall, 1997.
[21] R. Roy *et al.*, "ESPRIT and uniform linear arrays," in *Proc. 33rd SPIE Int. Technical Symp., Adv. Algorithms Architectures Signal Process. IV*, San Diego, CA, Aug. 1989, pp. 370–381.
[22] M. Goldburg and R. Roy, "Application of ESPRIT to parameter estimation from uniformly sampled data," in *Proc. IEEE ICASSP*, Albuquerque, NM, 1990.
[23] Y. Bresler and A. Delaney, "Resolution of overlapping echoes of unknown shape," in *Proc. IEEE ICASSP*, Glasgow, U.K., 1989, vol. 4, pp. 2657–2660.

Andreas Jakobsson received the M.Sc. degree in computer science and engineering from Lund Institute of Technology, Lund, Sweden, in 1993 and the Licentiate degree in signal processing from Uppsala University, Uppsala, Sweden, in 1997.

From 1994 to 1995, he was enrolled as a graduate nondegree student at the University of California, San Diego. During the Fall of 1996, he was a Visiting Researcher at Katholieke Universiteit Leuven, Leuven, Belgium, and during the Fall of 1997, he was with Stanford University, Stanford, CA. During 1998, he has been a Visiting Researcher at Brigham Young University, Provo, UT. Since 1995, he has been enrolled in the Ph.D. program at the Systems and Control Group, Uppsala University.

A. Lee Swindlehurst (M'90) received the B.S. degree (summa cum laude) and M.S. degree in electrical engineering from Brigham Young University (BYU), Provo, UT, in 1985 and 1986, respectively, and the Ph.D. degree in electrical engineering from Stanford University, Stanford, CA, in 1991.

From 1983 to 1984, he was employed with Eyring Research Institute, Provo, UT, as a Scientific Programmer, writing software for a Minuteman missile simulation system. From 1984 to 1986, he was a Research Assistant, Department of Electrical Engineering, BYU. He was awarded an Office of Naval Research Graduate Fellowship between 1985 and 1988, and during that time, he was affiliated with the Information Systems Laboratory, Stanford University. From 1986 to 1990, he was also employed at ESL, Inc., Sunnyvale, CA, where he was involved in the design of algorithms and architectures for a variety of radar and sonar signal processing systems. He joined the faculty of the Department of Electrical and Computer Engineering, BYU, in 1990, where he holds the position of Associate Professor. From 1996 to 1997, he held a joint appointment as a Visiting Scholar at both Uppsala University, Uppsala, Sweden, and at the Royal Institute of Technology, Stockholm, Sweden. His research interests include sensor array signal processing for radar and wireless communications, detection and estimation theory, and system identification.

Dr. Swindlehurst is a past Associate Editor of the IEEE TRANSACTIONS ON SIGNAL PROCESSING.

Petre Stoica (F'94), for photograph and biography, see p. 160 of the January 1998 issue of this TRANSACTIONS.